S-Domain Methods for Simultaneous Time and Frequency Characterization of Electromagnetic Devices

J. Eric Bracken, *Member, IEEE,* Din-Kow Sun, *Member, IEEE,* and Zoltan J. Cendes, *Member, IEEE*

Abstract— An efficient procedure is developed for simultaneously characterizing the time-domain and frequency-domain behavior of electromagnetic devices. The procedure works in the complex-frequency plane—called the s-domain—and provides an analytical expression for the behavior of the device at any frequency and for any transient excitation. This analytical expression is obtained by first evaluating a reduced-order model of the poles and zeros of the device. These poles and zeros are then used to characterize the device in terms of rational polynomials in the s-domain. Two different methods for evaluating reduced-order models are presented. One is called asymptotic waveform evaluation (AWE) and is combined with the finite-element method; the other is called adaptive Lanzcos–Padé sweep (ALPS) and is combined with the boundary-element method. The resulting reduced-order models provide the frequency-domain behavior of the device over a broad bandwidth. Using the Laplace transform, these reduced-order models also provide the time-domain behavior. Several numerical examples have been run using commercial electronic design automation (EDA) software to demonstrate that this solution procedure is a highly efficient and accurate way to characterize the electromagnetic performance of real-life devices.

Index Terms—Electromagnetic analysis, electromagnetic transient analysis, finite-element methods, Maxwell's equations, reduced-order systems.

I. INTRODUCTION

TIME-DOMAIN and frequency-domain procedures are often used to characterize passive linear electromagnetic devices. In a time-domain method, such as the finite-difference time-domain (FDTD) or transmission-line matrix (TLM) algorithms [1], Maxwell's equations are discretized in both space and time, and time stepping is used to compute the temporal evolution of the field throughout the solution region. In a frequency-domain method, such as the usual finite-element and boundary-element methods, Maxwell's equations are written in the frequency domain and the fields in the solution region are computed at a set frequency. In either case, problems must be solved over and over again to determine the transient response to a variety of different excitations, or to find the frequency response over a broad bandwidth.

This paper presents a different approach. We develop procedures to compute a reduced-order model of the transfer function of the passive linear electromagnetic system. This reduced-order model is derived in the complex-frequency plane called the s-domain. Since the response of a linear system is determined by its transfer function, once the reduced-order model is known, both the time-domain and frequency-domain response of the system can be computed without the need for additional field solution.

The transfer function of a linear system described by ordinary differential equations may be expressed as a rational polynomial in terms of its poles and zeros. For a system described by partial differential equations, such as electromagnetics, the number of poles and zeros is infinite. Thus, to be computationally tractable, we need to approximate this infinite set by computing only the dominant poles and zeros of the system. The resulting approximation to the transfer function is called a reduced-order model. Two different procedures exist in the literature for finding reduced-order models. One is called asymptotic waveform evaluation (AWE) [2]–[5] and the other is called the Padé via Lanczos (PVL) algorithm [6]. Both of these procedures were originally applied to the solution of electronic circuits; here we extend these procedures to make them suitable for electromagnetic analysis.

There are several advantages to the s-domain approach. First, the electromagnetic transfer function is computed only once. Since the system is linear, there is no need to compute electromagnetic fields over and over again by stepping either through time or frequency. Second, s-domain solutions are fast. Once the electromagnetic transfer function is computed, frequency sweeps and transient analyzes take only seconds or even fractions of a second. Third, the electromagnetic analysis may be performed by using either differential- or integral-equation methods. In this paper, we employ both the finite-element and boundary-element methods to compute the transfer function. Fourth, s-domain solutions may be converted into equivalent electrical circuits. These equivalent circuits can be combined with external voltage and current sources and the entire system modeled by using circuit simulators. Fifth, it is very easy to use these reduced-order models in "what-if" design variations. Since the electromagnetics are done once and for all, it is possible to pass these detailed models on to design groups working at the system level.

Early work on s-domain methods in electromagnetics was performed by Newman [7] and by Kottapalli *et al.* [8]. An AWE-based fast-sweep method for integral equations was

first presented in 1992 [9]. The first fast-sweep method that combined AWE with the finite-element method was presented in 1993 [10]. A improved form of the PVL algorithm called adaptive Lanzcos–Padé sweep (ALPS) for use with integral equations was presented in 1996 [11]. AWE has been employed in the finite-element-based electromagnetics simulation package high-frequency structure simulator (HFSS) to provide a fast frequency sweep capability since 1993.[1] ALPS has been employed in the boundary-element-based electromagnetics simulation package Maxwell Strata since 1996.[2]

This paper begins by introducing the two main approaches to s-domain analysis: AWE and PVL. We also develop improvements to these methods called complex frequency hopping (CFH) and ALPS. We then derive reduced-order models from the differential form of Maxwell's equations combining AWE with the finite-element method. This is followed by the generation of reduced-order models from the integral form of Maxwell's equations, combining ALPS with the boundary-element method. Finally, we develop procedures for obtaining transient results from reduced-order models. These transient results are obtained by creating circuit equivalents for the reduced-order models and computing the transient response via standard SPICE-like circuit simulators. The procedures are illustrated by real-life examples.

II. AWE

AWE begins by applying the Laplace transform to the linearized time-dependent Maxwell's equations. This converts Maxwell's equations into a form dependent on the complex frequency parameter s. Using the Laplace transform and numerical discretization, both the differential form or the integral form of Maxwell's equations can be written in the form

$$A(s)x(s) = b(s). \tag{1}$$

Here, $x(s)$ is a vector consisting of the desired solution quantities, i.e., electric and magnetic fields with differential methods, current densities, and charges with integral methods, $b(s)$ is a vector containing the contributions of applied sources, and $A(s)$ is the matrix generated by the discretization.

The impulse response of this linear system is defined as

$$H(s) = [A(s)]^{-1}bu(s) \tag{2}$$

where $u(s)$ is the Laplace transform of the unit impulse (Dirac delta) function and b is a constant column vector. For a finite-order system like a lumped circuit, this impulse response is a rational function

$$H(s) = \frac{\beta_0 + \beta_1 s + \beta_2 s^2 + \cdots + \beta_q s^q}{\alpha_0 + \alpha_1 s + \alpha_2 s^2 + \cdots + \alpha_q s^q}. \tag{3}$$

A rational $H(s)$ may also be written in the factored form

$$H(s) = \frac{\beta_q(s - z_q)(s - z_{q-1})\cdots(s - z_1)}{\alpha_q(s - p_q)(s - p_{q-1})\cdots(s - p_1)} \tag{4}$$

[1] *HFSS User Manual*, Hewlett-Packard Corporation, Santa Rosa, CA, and Ansoft Corporation, Pittsburgh, PA, 1993.
[2] *Maxwell Strata User Manual*, Ansoft Corporation, Pittsburgh, PA, 1996.

where the p_i and the z_i are the poles and zeros of the system, respectively.

We may, therefore, represent any component of the solution vector x_i by using a low-order rational function that is a good approximation over a certain frequency band to the exact (high-order) one. A well-known procedure for accomplishing this task is the Padé approximation [12]. The first $2q+1$ terms of the Taylor-series expansion for (2) about the point s_0 are computed [2], [3], [5] and matched to the Taylor coefficients of the reduced-order model. This results in

$$\begin{aligned} H(s) &= \sum_{n=0}^{2q} (s - s_0)^n \cdot xh_n \\ &= \frac{\beta_q(s-s_0)^q + \cdots + \beta_1(s-s_0) + \beta_0}{\alpha_q(s-s_0)^q + \cdots + \alpha_1(s-s_0) + \alpha_0}. \end{aligned} \tag{5}$$

This can be solved by cross-multiplying the denominator of the rational function and then equating terms with like powers of $(s - s_0)$. An approximation accurate over a broad frequency band can often be determined by computing just 10–20 terms of the Taylor-series expansion. Once we have a formula characterized in terms of just a few parameters a_i and b_i, it is a simple matter to evaluate the frequency response by substituting in a particular value of s.

III. CFH

It is shown in [6] that the recursion relation in AWE is equivalent to the power method for computing the eigenvectors of the matrix A. Since the power method converges most strongly to the largest eigenvector of the matrix A, this makes is difficult to compute many terms in the sequence accurately. Fortunately, in many cases, the number of poles q required to achieve a good approximation is very small. This is because the first few moments corresponding to the derivatives of the Taylor series contain the most information about the dominant poles and zeros of the system near the center frequency ω_0. Initially, as the number of terms in the Taylor series increases, the bandwidth over which an accurate solution is obtained also increases. The higher order terms are more difficult to compute because of the nature of the power method and the finite precision of the computer. Numerical simulations reveal that increasing the number of poles beyond 10 or 12 does not necessarily improve the accuracy of the approximation at frequencies that are far away from the center frequency.

As a remedy to the above problem, a procedure called CFH may be used [5]. In this procedure, the moments are computed at multiple frequencies. A single rational function is then derived, which is valid over a wider bandwidth by combining the results obtained at the multiple frequencies.

To perform CFH, we seek a rational function in the form

$$\hat{H}(s) = \frac{\sum_{i=0}^{q-1} b_i \left[\frac{j}{\omega_0}(s - j\omega_0) \right]^i}{\sum_{i=0}^{q} a_i \left[\frac{j}{\omega_0}(s - j\omega_0) \right]^i}. \tag{6}$$

Assuming $a_0 = 1$, (6) becomes

$$\hat{H}(s) = \sum_{i=0}^{q-1} b_i \left[\frac{j}{\omega_0}(s - j\omega_0) \right]^i - \sum_{i=1}^{q} a_i \hat{H}(s) \left[\frac{j}{\omega_0}(s - j\omega_0) \right]^i.$$

(7)

The kth derivative of (7) at frequency $s = j\omega_j$ is obtained as

$$\hat{H}^{(k)}(j\omega_j) = \sum_{i=k}^{q-1} \frac{b_i i!}{(i-k)!} \left(\frac{j}{\omega_0} \right)^k \left[\frac{-1}{\omega_0}(\omega_j - \omega_0) \right]^{i-k}$$
$$- \sum_{i=1}^{q} a_i \sum_{n=0}^{\min(i,k)} \frac{i!k!}{n!(i-n)!(k-n)!} \left(\frac{j}{\omega_0} \right)^n$$
$$\cdot \hat{H}^{(k-n)}(j\omega_j) \left[\frac{-1}{\omega_0}(\omega_j - \omega_0) \right]^{i-n}.$$

(8)

This can be rewritten as

$$\left(\frac{\omega_0}{\omega_j} \right)^k \overline{H}^{(k)}(j\omega_j) = \sum_{i=k}^{q-1} \frac{b_i i!}{(i-k)!k!} \left[\frac{-1}{\omega_0}(\omega_j - \omega_0) \right]^{i-k}$$
$$- \sum_{i=1}^{q} a_i \sum_{n=0}^{\min(i,k)} \frac{i!}{n!(i-n)!} \left(\frac{\omega_0}{\omega_j} \right)^{k-n}$$
$$\cdot \overline{H}^{(k-n)}(j\omega_j) \left[\frac{j}{\omega_0}(\omega_j - \omega_0) \right]^{i-n}$$

(9)

where

$$\overline{H}^{(k)} = \left(\frac{\omega_j}{j} \right)^k \frac{\hat{H}^{(k)}(j\omega_j)}{k!}.$$

(10)

Equations (9) and (10) have been scaled appropriately to improve numerical stability.

If the number of frequency points is N and the number of derivatives at ω_j is K_j, then a matrix equation for the coefficients in (6) can be generated using (9) as long as $\sum_{j=1}^{N}(K_j - 1) > (2q + 1)$. A rational function providing a continuous interpolation between several frequency points is thus obtained. As a result, the bandwidth over which an accurate approximation is obtained is much wider than a single frequency Padé approximation. The spectral response can also be much more complex.

A measure of the quality of the Padé approximation is provided by the matrix residual

$$\text{Error}(s) = \frac{\|A(s)x(s) - b(s)\|}{\|b(s)\|}$$

(11)

where $A(s)$ and $b(s)$ are the same as in (1). Computing this matrix residual is very efficient because the matrix vector multiplication involves the finite-element coefficient matrix, which is very sparse. The residual computation consumes far less central processing unit (CPU) time than is required for matrix decomposition and provides a good indicator of the accuracy of the solution. A large matrix residual indicates a poor solution. The minimum residual always occurs at the center frequency ω_0, where the residual is theoretically zero.

As the difference between ω and ω_0 increases, the residual also increases.

While the Padé approximation was performed above with the s-parameters of the electromagnetic circuit, a similar procedure can be used with every element of the vector $x(s)$. This means the electromagnetic-field behavior is also captured by using the AWE process. At first, this would seem to be a daunting task since the finite-element solution vector is usually large. However, every element of the solution vector has the same poles, while the zeros can be obtained by simple summation. Thus, the difficulty is illusory and we can readily plot complete electromagnetic-field data at any frequency from an s-domain solution. Indeed, the computer program HFSS allows users to plot electromagnetic fields at any frequency within the solution bandwidth from a single center frequency solution.[1]

IV. ALPS

To avoid the numerical instabilities in AWE, Feldmann and Freund have developed a procedure called PVL [6]. PVL has the advantage of using the numerically robust Lanczos algorithm to compute the eigenvalues of the system, rather than the more problematic power method. It also has the benefit of providing error estimates of the resulting poles and zeros.

The relationship between AWE and the eigenvalues of the system is explained in [13]. Assuming that the frequency dependence of the system matrix $A(s)$ can be separated as $A(s) = A_0 + sA_1$ (where A_0 and A_1 are frequency independent matrices), we can rewrite (2) as

$$H(s) = (I - sM)^{-1} r(s)$$

(12)

where $M = -A_0^{-1} A_1$ and $r(s) = A_0^{-1} bu(s)$. Diagonalize the matrix M as

$$M = \chi \Lambda \chi^{-1}$$

(13)

where χ are the eigenvectors of M and $\Lambda = \text{diag}(\lambda_1, \lambda_2, \cdots, \lambda_N)$ is the matrix of eigenvalues λ_i. Then (12) can be written as

$$H(s) = \chi(I - s\Lambda)^{-1} \chi^{-1} r(s).$$

(14)

This gives

$$H(s) = \sum_{i=1}^{N} \frac{\xi_i \cdot \rho_i}{1 - s\lambda_i}$$

(15)

where ξ_i and ρ_i are the ith row in χ and the ith column in $\chi^{-1} r(s)$, respectively.

Equation (15) shows that the impulse response of a linear system can be treated as an eigenvalue problem and that the system poles are related to its eigenvalues. In theory, determining the system response requires that all of the eigenvalues of the matrix M be computed. However, in practice, it is sufficient to compute only the eigenvalues in or near the desired frequency range. This leads us to the Lanczos algorithm. Consider the generalized eigenvalue problem

$$A_1 \chi = -A_0 \chi \Lambda$$

(16)

which has been derived from (13). The Lanczos algorithm approximates the eigenvalues of a large-dimensional matrix pair (A_0, A_1) with a sequence of small-dimensional matrix pairs (T_k, I), $k = 2, 3, \cdots, N$, where T_k is a tridiagonal matrix of dimension k. The eigenvectors of this ever-growing sequence are in a vector space called a *Krylov subspace*. Details of this process are given in [14].

Although PVL is more stable than AWE, the Krylov vectors thus generated eventually lose orthogonality and the method stagnates. Sun has proposed a robust alternative to PVL based on Arnoldi iteration as modified by Parlett *et al.* [15], [16]. In the original Arnoldi process, the newly computed Krylov vector must be kept orthogonal to all previous Krylov vectors. This requirement is expensive and limits the method to small problems. However, Parlett and Scott showed that Krylov vectors lose their mutual orthogonality only when the Lanczos process converges to an eigenvector of the system [15]. By employing a measure to identify whether or not a Krylov vector has converged to an eigenvector, newly computed Krylov vectors only need to be kept orthogonal to the set of converged eigenvectors. This is called selective orthogonalization and is much more efficient than the original approach. Compared to PVL, the new algorithm is not only numerically stable, but is also more efficient since it takes only one matrix–vector multiplication per Lanczos iteration and it simultaneously computes the multioutput parameters for a single input. Even when the computer runs out of storage for the Krylov and other vectors, one still obtains a spectral solution for a smaller frequency range. One can restart at another frequency to obtain the remaining spectral solution.

In the above, we assumed that quadratic and higher order terms do not contribute to the Taylor-series expansions (2). This is not entirely true, although these terms may be neglected if the frequency range is small enough. To obtain a wide-band response, we employ an adaptive process. Suppose that we are interested in the spectral-domain response in the band $[f_{\min}, f_{\max}]$. We first compute two different reduced-order models using $f_{\min}$ and $f_{\max}$ as two different center frequencies. We then compute the spectral response of the system throughout the entire band $[f_{\min}, f_{\max}]$ using both reduced-order models. If the two response are within an acceptable error tolerance throughout $[f_{\min}, f_{\max}]$, then the procedure has converged. However, if the two responses differ by more than the error tolerance, the frequency of maximum error $f_{\max}$ is noted. An additional reduced-order model is then computed using $f_{\max}$ as a new center frequency, and the error checking process is repeated in the two new subintervals. This process is repeated until the two reduced-order models bordering all subintervals give the same spectral response to within the set error tolerance. The several resulting reduced-order models are then combined to form a single higher order reduced-order model using the procedures described n Section III.

V. THE TRANSFINITE-ELEMENT METHOD

The time-dependent Maxwell's equations in stationary source-free regions are

$$\nabla \times \vec{\mathbf{E}} = -\mu \frac{\partial}{\partial t} \vec{\mathbf{H}} \tag{17}$$

$$\nabla \times \vec{\mathbf{H}} = \varepsilon \frac{\partial}{\partial t} \vec{\mathbf{E}} + \sigma \vec{\mathbf{E}} \tag{18}$$

where $\vec{\mathbf{E}}$ and $\vec{\mathbf{H}}$ are the time-domain electric and magnetic fields, respectively and μ, ε, and σ are the material permeability, permittivity, and conductivity, respectively. Equations (17) and (18) are solved directly in procedures such as the FDTD and TLM algorithms. Maxwell's equations in the s-domain are obtained by taking the Laplace transform of (17) and (18), assuming zero initial conditions, and rearranging terms

$$\nabla \times \vec{E} = -\mu(s - s_0)\vec{H} - \mu s_0 \vec{H} \tag{19}$$
$$\nabla \times \vec{H} = \varepsilon(s - s_0)\vec{E} + (\epsilon s_0 + \sigma)\vec{E} \tag{20}$$

Here $\vec{E}$ and $\vec{H}$ are the Laplace transforms of $\vec{\mathbf{E}}$ and $\vec{\mathbf{H}}$, respectively, and s_0 is an arbitrary complex frequency. To increase computational efficiency, we eliminate either $\vec{E}$ or $\vec{H}$ by combining (19) and (20) to give a vector-wave equation. In the following, we generate the vector-wave equation in $\vec{E}$; a similar procedure can be used to generate an equation in $\vec{H}$. Taking the curl of (19) and using (20) gives

$$\nabla \times \frac{1}{\mu} \nabla \times \vec{E} + s_0^2 \left(\varepsilon + \frac{\sigma}{s_0} \right) \vec{E}$$
$$= -\varepsilon(s - s_0)^2 \vec{E} - (s - s_0)(2\varepsilon s_0 + \sigma)\vec{E}. \tag{21}$$

Setting $s_0 = j\omega_0$ and scaling both sides by μ_0 yields

$$\nabla \times \frac{1}{\mu_r} \nabla \times \vec{E} + k_0^2 \varepsilon_r' \vec{E}$$
$$= -\frac{1}{\omega_0^2} [\varepsilon_r(s - j\omega_0)^2 + 2j\omega_0 \varepsilon_r''(s - j\omega_0)]k_0^2 \vec{E} \tag{22}$$

where $k_0 = \omega_0 \mu_0 \varepsilon_0$ is the wavenumber at frequency ω_0, and ε_r' and ε_r'' are the complex relative dielectric constants

$$\varepsilon_r' = \varepsilon_r - j\frac{\sigma}{\omega_0 \varepsilon_0} \tag{23}$$
$$\varepsilon_r'' = \varepsilon_t - j\frac{\sigma}{2\omega_0 \varepsilon_0}. \tag{24}$$

Note that the electric field in (22) is a function of the complex frequency s relative to the center frequency ω_0.

The transfinite-element method uses a combination of finite elements and mode matching to compute the electromagnetic field [17]. Consider an arbitrary N-port three-dimensional microwave device enclosing a domain Ω, bounded by perfect conducting walls $\delta\Omega$, and having N-ports Γ_i, $i = 1, 2, \cdots, N$, illustrated in Fig. 1 with a two-port.

In this case, the boundary conditions associated with (22) for an arbitrary N-port structure are written as follows:

$$\hat{n} \times \vec{E} = 0 \quad \text{on} \quad \partial\Omega \tag{25}$$
$$\vec{E} = \vec{E}^{\text{inc}} + \sum_{j=1}^{M_i} S^i j \vec{e}_j^i \quad \text{on } \Gamma_i \tag{26}$$
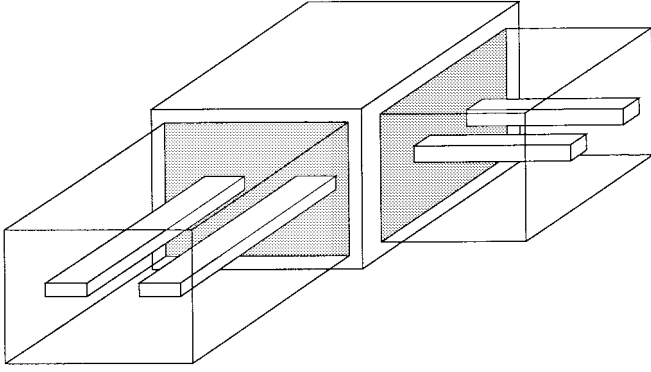
Fig. 1. Three-dimensional "black-box" fed by two triaxial cables.

$$\vec{E} = \sum_{j=1}^{M_k} S^k j \vec{e}_j^k \quad \text{on } \Gamma, \qquad k = 1, 2, \cdots, N, \; k \neq i. \tag{27}$$

In (26) and (27), $\vec{E}^{\text{inc}}$ is the incident electric field and $\vec{e}_j^k$ is the electric field mode of the jth mode on the kth port. In the transfinite-element method, the incident field is taken to be one of the eigenmodes, and all eigenmodes are normalized to give unity Poynting vector

$$\oint_{\Gamma_i} (\vec{e}_j^i \times \vec{h}_j^i) \cdot \hat{n}_i d\Gamma = 1. \tag{28}$$

It can be shown that the coefficients S_j^k are the same as the elements of the N-port generalized scattering matrix [17]. The s-parameters computed in the transfinite-element method are variationally stationary and converge faster than the electric field. This allows them to be computed very accurately.

Following the procedures in [17]–[19], we expand the electric field as

$$\vec{E} = \sum_{j=1}^{N_e} E_j \vec{\gamma}_j \tag{29}$$

where $\vec{\gamma}_j$ are tangential-vector finite elements. Applying Galerkin's method generates the s-domain transfinite-element matrix equation

$$(A^{(1)} + \Psi)x(s)$$
$$= \frac{j}{\omega_0} \Big[(s - j\omega_0)^2 A^{(2)} + (s - j\omega_0)A^{(3)} \Big] x(s)$$
$$- b^{(1)} + \frac{j}{\omega_0} \Big[(s - j\omega_0)^2 b^{(2)} + (s - j\omega_0)b^{(3)} \Big]. \tag{30}$$

Note that (30) provides the dependence on the complex frequency s explicitly. The matrices in (30) assume different forms depending on the number of ports. For simplicity, we present the expressions here for a two-port. Let I stand for the interior unknowns, Γ_1 stand for the unknowns on port 1, Γ_2 stand for unknowns on port 2, P_1 and P_2 contain the tangential electric fields on ports 1 and 2, respectively, P_1^T

stand for the transpose of P_1, Ψ_1 and Ψ_2 are the input power on ports 1 and 2, respectively, and $\{\vec{\gamma}_i, \; i = 1, 2, \cdots, N_e\}$ are a set of tangential-vector finite elements, where N_e is the total number of vector basis functions used in approximating the electric field. In this case, the matrices in (30) may be written as

$$A^i = \begin{bmatrix} M_{II}^i & M_{I\Gamma_1}^i P_1 & M_{I\Gamma_2}^i P_2 \\ P_1^T M_{\Gamma_1 I}^i & P_1^T M_{\Gamma_1 \Gamma_1}^i P_1 & P_1^T M_{\Gamma_1 \Gamma_2}^i P_2 \\ P_2^T M_{\Gamma_1 I}^i & P_2^T M_{\Gamma_2 \Gamma_1}^i P_1 & P_2^T M_{\Gamma\Gamma_2}^i P_2 \end{bmatrix} \tag{31}$$

$$\Psi = \begin{bmatrix} 0 & 0 & 0 \\ 0 & \Psi_1 & 0 \\ 0 & 0 & \Psi_2 \end{bmatrix} \tag{32}$$

$$M_{ij}^1 = \left\langle \nabla \vec{\gamma}_i \mid \frac{1}{\mu_r} \nabla \times \vec{\gamma}_j \right\rangle - \langle \vec{\gamma}_i \mid \vec{\gamma}_j \rangle \tag{33}$$

$$M_{ij}^2 = -2k_0^2 \frac{\langle \vec{\gamma}_i \mid \varepsilon_r' \vec{\gamma}_j \rangle}{2j\omega_0} \tag{34}$$

$$M_{ij}^3 = -2k_0^2 \langle \vec{\gamma}_i \mid \varepsilon_r'' \vec{\gamma}_j \rangle. \tag{35}$$

The solution vector $x(s)$ contains the electric field and the scattering parameters S_j^k. For a two-port, it is

$$x(s) = \begin{bmatrix} E_I^1 & E_I^2 \\ s_{11} & s_{21} \\ s_{12} & s_{22} \end{bmatrix}. \tag{36}$$

The right-hand sides $b^{(i)}$ in (30) all have the same structure. For a two-port device, $b^{(i)}$ has two columns and is given by

$$b^{(i)} = \begin{bmatrix} b_1^i & b_2^i \end{bmatrix} \tag{37}$$

where

$$b_k^i = \begin{bmatrix} M_{I\Gamma_k}^i P_k \\ P_1^T M_{\Gamma_k \Gamma_1}^i P_k - \gamma_{11}^i \\ P_2^T M_{\Gamma_k \Gamma_2}^i P_k - \gamma_{22(11)}^i \end{bmatrix}. \tag{38}$$

Here the matrix γ is nonzero only in b^1.

The domain Ω of the structure may contain arbitrary conductors and materials. The tangential-vector finite elements ensure the tangential continuity of the electric field and provide for the continuity conditions between materials through the natural boundary conditions in the variational principle. Impedance boundary conditions may be set on lossy conductors, zero tangential electric field is set on perfect conductors, and absorbing boundary conditions are set on open radiating boundaries.

VI. THE MIXED-POTENTIAL INTEGRAL EQUATION

The following development is similar to that presented in [8] and [24], so here we will be brief. To apply the s-domain method to integral equations, we write with the mixed-potential integral equation in terms of the unknown distribution of surface currents $\vec{J}(\vec{r})$.

$$s\hat{n} \times \vec{E}^{\text{inc}} = -\hat{n} \times \Big[s^2 \int_{S'} \overline{G}_A(\vec{r}, \vec{r}') \cdot \vec{J}(\vec{r}') da' $$
$$+ \nabla \int_{S'} G_\phi(\vec{r}, \vec{r}') \nabla' \cdot \vec{J}(\vec{r}') da' \Big]. \tag{39}$$

Here, $\overline{G}_A$ represents the dyadic Green's function for the vector potential, G_ϕ represents the scalar Green's function, and $\hat{n}$ is the unit vector normal to the surface at the field observation point $\vec{r}$. We assume that the only objects in the problem are perfect electrical conductors, so that the sum of the incident and scattered electric fields is normal to the surface.

Now approximate $\vec{J}$ in (39) with Rao–Wilton–Glissen (RWG) basis functions $\{\vec{\beta}_j\}$ [27]

$$\vec{J} = \sum_{j=1}^{n} J_j \vec{\beta}_j. \tag{40}$$

Applying Galerkin's method provides

$$[K(s) + s^2 M(s)]J = sE \tag{41}$$

where

$$K_{ij} = \int_S \int_{S'} (\nabla \cdot \vec{\beta}_i) G_\phi(\vec{r}, \vec{r}')(\nabla' \cdot \beta_j) da' da$$

$$M_{ij} = \int_S \int_{S'} \vec{\beta}_i \cdot \overline{G}_A(\vec{r}, \vec{r}') \cdot \beta_j da' da$$

$$E_i = \int_S \vec{\beta}_i \cdot (\hat{n} \times \vec{E}^{\text{inc}}) da. \tag{42}$$

Although the matrices K and M depend on frequency through the Green's functions, we assume for the moment that they do not. This allows us to make a change of variables $b = sE$ and $u = s^2$ to express (41) as

$$(K + uM)J = b. \tag{43}$$

The ALPS procedure described in Section IV may then be applied to find a piecewise rational-function approximation to the frequency response over the band of interest.

VII. REDUCED-ORDER MODELS

Given a frequency response $f(s)$, it is desirable to create a single rational-function model valid across a wide frequency band. If this can be achieved, then it is a simple matter to transform the response of the system back to the time domain. This time-domain representation can be simulated efficiently in SPICE-like programs using recursive convolution techniques [29].

To compute such a model, we use rational-function interpolation, pole pruning, and least-squares fitting. The initial "unconstrained" rational-function interpolation procedure [20] is carried out in order to find a model that passes through the computed data at a set of equally spaced points along the line $s = j\omega$. To choose the interpolant's order, we start with a small number of interpolation points and then increase the number of points until an acceptably accurate fit is achieved between the interpolation points.

The unconstrained interpolation procedure may produce nonphysical, unstable right-half-plane poles. In the pole-pruning stage, these poles are eliminated from the model. This makes the model stable, but introduces additional approximation errors. To minimize these errors, a final least-squares fitting procedure is used to adjust the residues $\{k_i\}$ of the remaining poles. Typically, we find that a maximum error of about 1% is achievable with 5–30 poles.

In order to carry out simulation of complete digital or microwave circuits, it is desirable to include both the electromagnetic effects of interconnects as well as the nonlinear effects of transistors and diodes. Thus, we wish to incorporate the reduced-order models we have derived within circuit simulation packages such as SPICE [21], [22]. The main challenge in doing this is translating between the scattering parameter models of high-frequency electromagnetics and the circuit models of SPICE.

In order to communicate with a circuit simulator, we must develop a relationship between the modal fields and certain "voltage" and "current" signals. In circuit theory, the voltages are typically defined as potential differences between each signal conductor and a "ground" conductor. In electromagnetics, it is more common to work with the power-scattering matrix S

$$b = Sa. \tag{44}$$

This relates the intensities of the incident and reflected waveguide modes at each port. We seek a similar relationship defined in terms of signal voltages v and currents i. The desired relationship is called the pseudoscattering matrix S_p

$$b_p = S_p a_p \tag{45}$$

where the quantities a_p and b_p are the incident and reflected pseudowave intensities, defined as

$$a_p = \frac{1}{2}\left(Z_{\text{ref}}^{-1/2} v + Z_{\text{ref}}^{1/2} i\right)$$

$$b_p = \frac{1}{2}\left(Z_{\text{ref}}^{-1/2} v - Z_{\text{ref}}^{1/2} i\right). \tag{46}$$

Here, Z_{ref} is a diagonal matrix whose entries are the reference impedances for each circuit port. These reference impedances may be chosen arbitrarily; for simplicity, we demand that they be positive real numbers.

Formally, a voltage v_m is the integral of the transverse electric field $\vec{E}_t$ over an open path C_m

$$v_m = -\int_{C_m} \vec{E}_t(x, y) \cdot dl. \tag{47}$$

If the transverse electric field can be represented in terms of incident and reflected waveguide modes with intensities a_n and b_n, respectively, we then have

$$\vec{E}_t = \sum_n a_n \vec{e}_n(x, y) + \sum_n b_n \vec{e}_n(x, y).$$

Therefore, in terms of modal intensities, the voltage v_m becomes

$$v_m = \sum_n a_n t_{mn} + \sum_n b_n t_{mn}$$

where $t_{mn} = -\int_{C_m} \vec{e}_n(x, y) \cdot dl$ is an integral of the modal electric field.

Collecting all of the voltages and wave intensities together as vectors, the relationship becomes

$$v = T(a + b) \tag{48}$$

where $T = [t_{mn}]$ is a square matrix (4×4 for the structure in Fig. 1) defining the transformation from mode intensities to
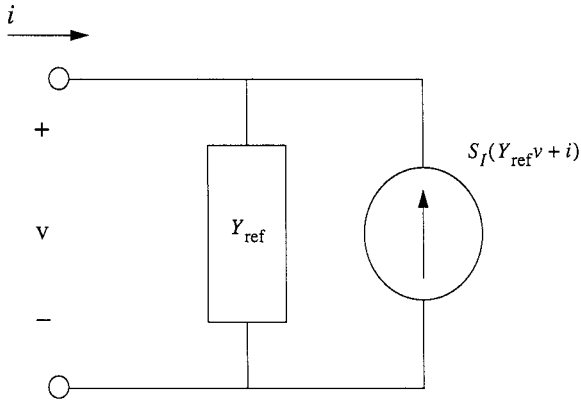
Fig. 2. A circuit interpretation of the current scattering relationship in (53).

Fig. 3. A microstrip T-junction.

port voltages. We need another such transformation to compute the port currents. The form of the relationship we seek is

$$i = U(a - b) \quad (49)$$

where $U = [u_{mn}]$ is a matrix relating modal intensities to currents. By demanding energy conservation between the circuit and electromagnetic models, it can be shown that

$$U^H T = P \quad (50)$$

where $P = [p_{mn}]$ is a matrix whose entries are the cross-power terms between the different waveguide modes

$$p_{mn} = \int_{\text{ports}} \vec{e}_m \times \vec{h}_n^* \cdot d\vec{S}. \quad (51)$$

The currents v and i can now be determined from the modal intensities a and b. By rearranging (46) and solving for b_p in terms of a_p, we can derive the desired pseudoscattering relation

$$S_p = [R(I + S)(I - S)^{-1}PR^H + I]^{-1}$$
$$\cdot [R(I + S)(I - S)^{-1}PR^H - I] \quad (52)$$

where $R = Z_{\text{ref}}^{-1/2}T$.

VIII. IMPLEMENTATION OF REDUCED-ORDER MODELS IN CIRCUIT SIMULATION

Using (46a), we can rewrite the pseudoscattering relationship $b_p = S_p a_p$ in terms of voltages and currents

$$Y_{\text{ref}}v - i = S_I(Y_{\text{ref}}v + i), \quad \text{where } S_I = Z_{\text{ref}}^{-1/2}S_p Z_{\text{ref}}^{1/2}. \quad (53)$$

We introduce $Y_{\text{ref}} = Z_{\text{ref}}^{-1}$ as well as the current-scattering matrix S_I. The advantage of (53) is that it lends itself to direct implementation in a circuit simulator. An equivalent circuit model for this relationship is shown in Fig. 2. The overall procedure for producing the equivalent circuit is summarized as follows.

1) Run an electromagnetic analysis on the structure of interest, using fast-sweep methods to find the modal scattering-parameter matrix S over a broad frequency band.
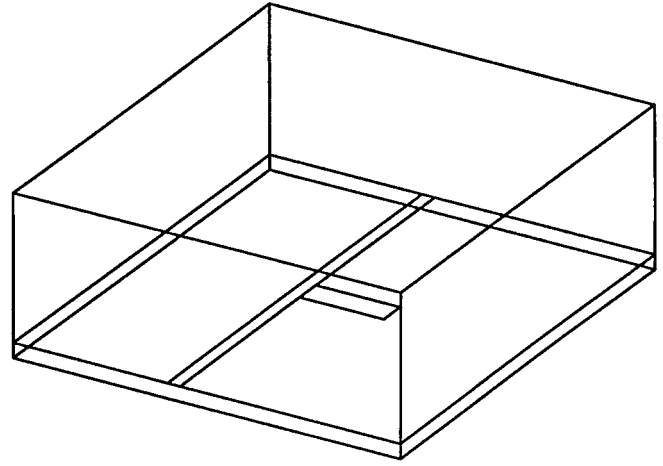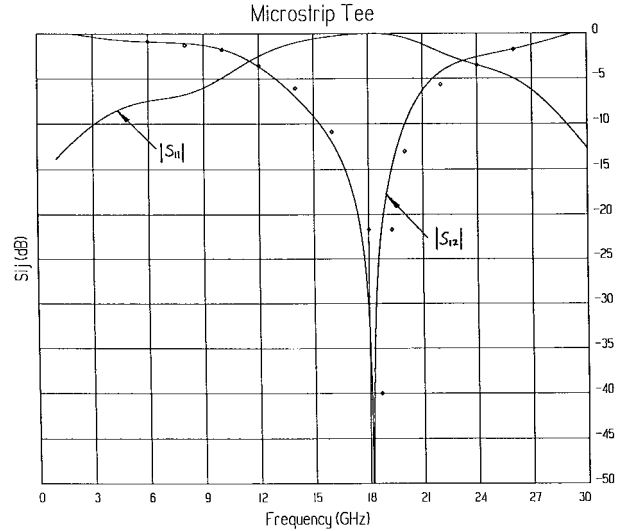

Fig. 4. Scattering parameters for the T-junction of Fig. 3. Solid line: calculated using AWE-based fast frequency sweep. Diamonds: measured results from [22].

2) Determine the transformation matrix X from the modal field patterns at the ports.
3) Compute the pseudoscattering matrix S_p and then convert it into a current-scattering matrix S_I.
4) Perform reduced-order modeling on the entries of the current-scattering matrix.
5) Write out the reduced-order models as frequency-dependent controlled sources in the form of a circuit deck for SPICE [21].

IX. NUMERICAL RESULTS

Consider first the microstrip T-junction of [23]. The substrate is 0.0254-cm-thick and has a relative dielectric constant of 9.9. The microstrip is 0.023-cm-wide and is assumed to
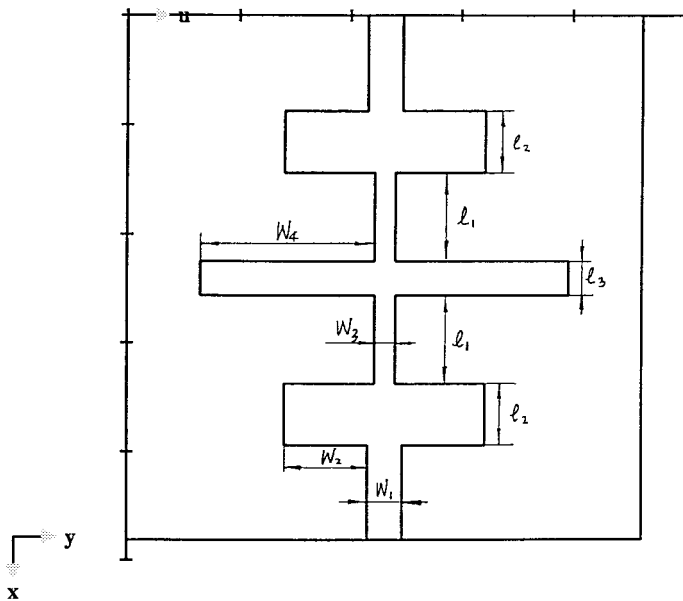
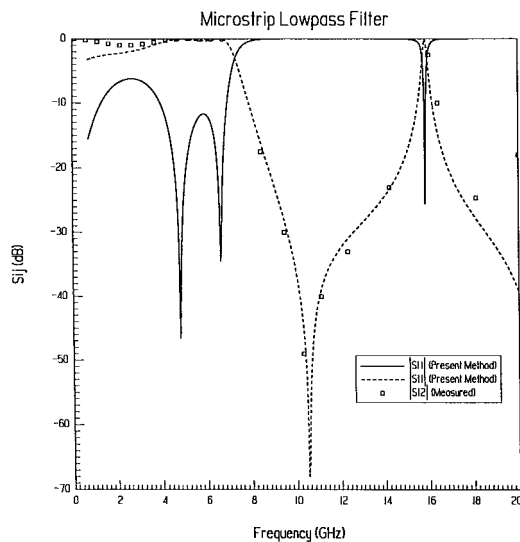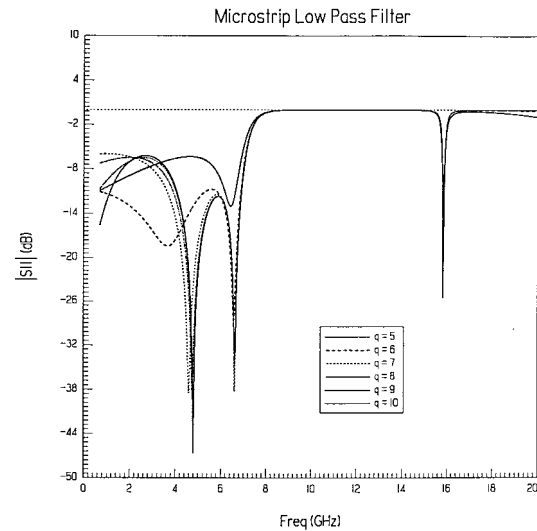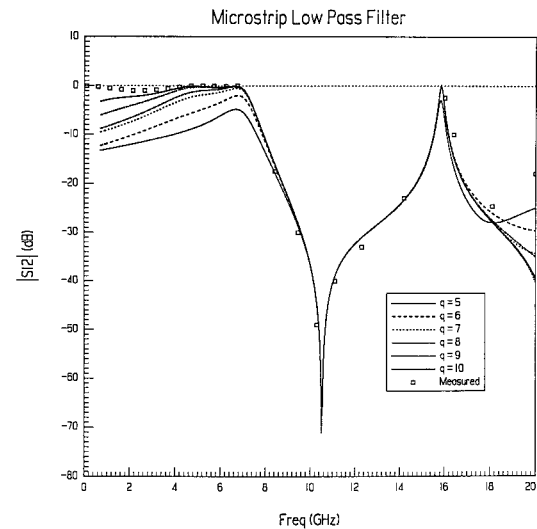Fig. 5. A three-pole microstrip filter design.

Fig. 7. Impact of the number of poles q in the AWE approximation on the return loss for the filter of Fig. 5.

Fig. 6. Comparison of scattering parameters for the filter of Fig. 5. Solid lines: AWE sweep results. Boxes: measured data.

Fig. 8. Impact of the number of poles q on the transmission coefficient for the filter of Fig. 5.

not know the location of the resonance ahead of time. In contrast, this resonance is accurately and easily computed by the s-domain method.

To illustrate the efficiency of the s-domain method, consider the microstrip low-pass filter, shown in Fig. 5. The dimensions of the filter are: $l_1 = 65$ mil, $l_2 = 45$ mil, $l_3 = w_1 = 25$ mil, $w_2 = 60$ mil, $w_3 = 15$ mil, and $w_4 = 125$ mil. The dielectric substrate has a relative dielectric constant of 9.6- and is 25-mil-thick. Fig. 6 compares this solution with measured results. Again, the agreement is excellent. Even though the spectral response of this filter is relatively complex, a single matrix solution at 12 GHz and 10 poles (20 additional forward/backward substitutions) are sufficient to obtain very accurate results over the wide band from 2 to 20 GHz. The matrix size used in this example was 63 214. The CPU time[3]

have zero thickness. The microstrip stub is 0.051-cm-wide and 0.153-cm-long. The geometry and computed numerical results are shown in Figs. 3 and 4. As shown in Fig. 4, the agreement between this theory (solid lines) and the measured results (markers) obtained by Giannini *et al.* [23, Fig. 17(a)] is very good. The s-domain method performs a single-matrix *LU* decomposition at 16 GHz and 16 additional forward and backward substitutions (i.e., eight poles are used in the Padé approximation) and accurately predicts the spectral response over the 3–30-GHz bandwidth. In contrast, with the frequency-domain method, one would have to solve the matrix equation at many discrete frequencies to obtain a similar frequency response curve. Capturing the resonant frequency near 18 GHz is not trivial with the frequency-domain method if one does

[3] These simulations were performed on an HP 9000/720 workstation with 64-MB RAM.
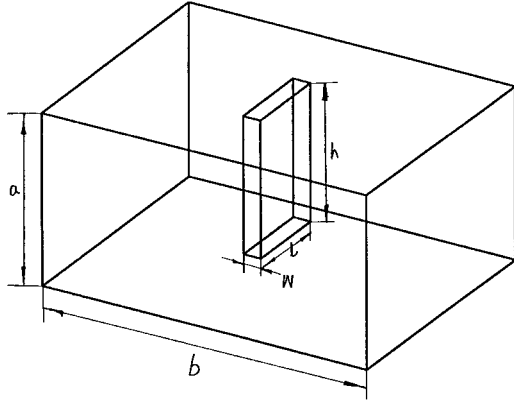
Fig. 9. A rectangular waveguide with a ridge discontinuity.

Fig. 12. Impact of the number of poles q in the AWE approximation on the return loss for the waveguide of Fig. 9. Also shown (x) are the "discrete" frequency sweep results.
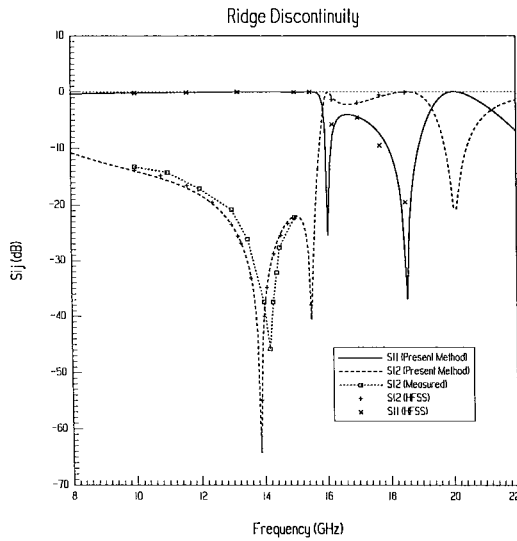

Fig. 10. The scattering parameters for the waveguide discontinuity of Fig. 9. The figure compares the AWE-based fast frequency sweep with measured data from [23].
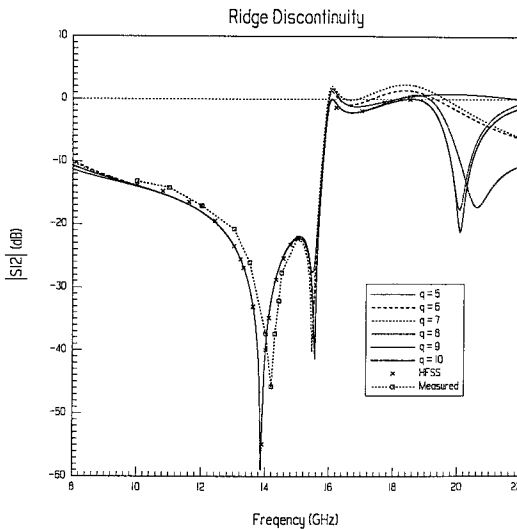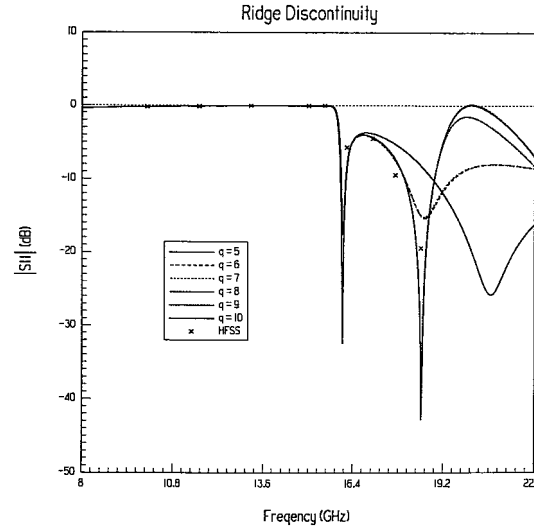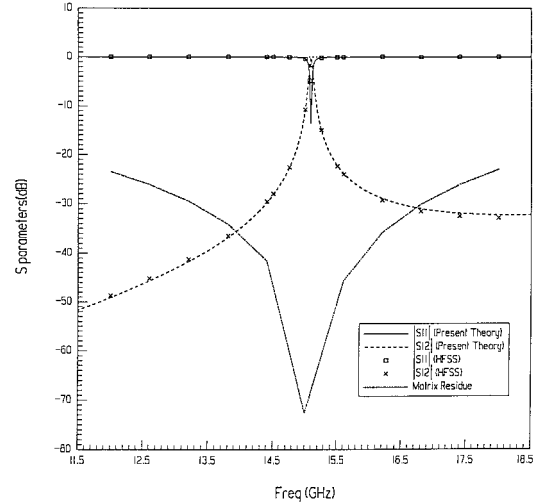

Fig. 13. Scattering parameters for the cross-iris problem of Fig. 13. AWE fast-sweep results are compared with HFSS discrete sweep results. Also shown is the matrix residual versus frequency.

Fig. 11. Impact of the number of poles q in the AWE approximation on the transmission coefficient for the waveguide of Fig. 9. Also shown (x) are the "discrete" frequency sweep results.

required to perform a single LU decomposition was 107.5 min. However, it requires only 7.4 CPU min to perform a single forward/backward substitution. Thus, LU decomposition takes 14 times more CPU time than forward and backward substitutions for this structure. Including the overhead of setting up this problem, the total CPU time for a single frequency point is $123.5 + 20 \times 7.4 = 271.5$ min. In contrast, if one were to solve the problem at 20 discrete frequencies, the total CPU time would be $20 \times 123.5 = 2470$ min. Thus, the s-domain method is approximately nine times faster and provides an analytic function for the spectral response versus the 20 discrete points obtained in the traditional method. With a spectral response as complicated as the one shown in Fig. 6, this analytical function is much more suitable for use in a microwave circuit simulation than are the 20 discrete values that must often be interpolated.
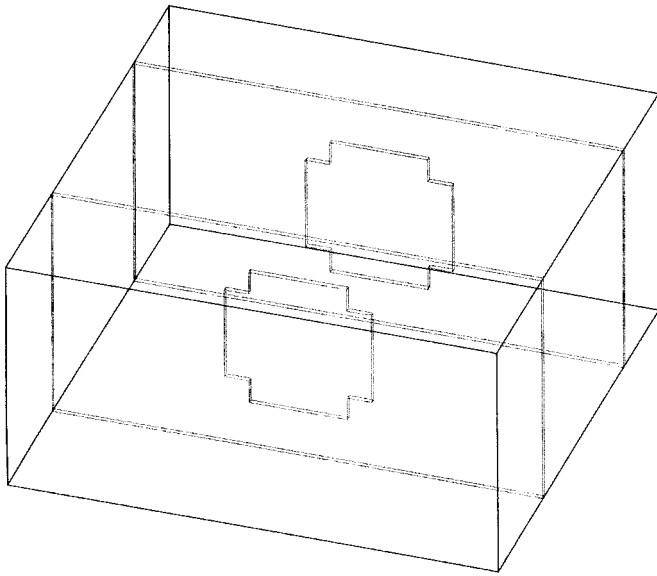
Fig. 14.   A rectangular waveguide with two cross irises.

Fig. 15.   Effect of the center frequency on the fast-sweep approximation for the waveguide cross-iris problem of Fig. 13.

Fig. 16.   An E-plane slot-coupled T-junction between two rectangular waveguides.

Figs. 7 and 8 illustrate the rate of convergence of the scattering parameters in terms of the number of poles used in the Padé approximation. The spectral response between 8 and 18 GHz is correctly captured with as few as five poles. This indicates that the dominant poles that produces the peaks and valleys in the response are already contained in the five-pole approximation. Additional poles improve the accuracy of the solutions at frequencies far away from the center frequency about the Taylor-series expansion point.

As a third example, consider the rectangular waveguide discontinuity, shown in Fig. 9. The waveguide is 19.05-mm-wide and 9.524-mm-high. The rectangular iris is centered with dimensions $w = 1.016$ mm, $l = 5.08$ mm, and $h = 7.619$ mm. Fig. 10 compares the numerical scattering parameters with measured results obtained by Mansour *et al.* [24, Fig. 6]. Figs. 11 and 12 again demonstrate the rate of convergence in terms of the number of poles used in the Padé approximations. With the center frequency at 13.0 GHz and five poles in the Padé approximation, the s-parameters are obtained accurately within the 10–15-GHz bandwidth. Adding poles to bring the reduced-order model up to ten poles produces accurate solutions between 8–22 GHz. The latter set of results is confirmed by using the Ansoft (HFSS) to perform a conventional "discrete" frequency sweep.

The above three examples clearly demonstrate the power and the limitations of the s-domain method. It is evident that the solution is most accurate over a limited bandwidth. The range of this bandwidth depends on the number poles used in the model and on the complexity of the spectral response. Since the Padé approximation only catches dominant poles and zeros, the accuracy bandwidth decreases with increasing complexity in the spectral response. the global matrix-residue error criterion in (11) indicates the range of validity of the Padé approximation. Fig. 13 presents the matrix residue plot for the rectangular waveguide cross-iris problem shown in Fig. 14. For this example, the minimum residue is located at the center frequency of 15 GHz where only roundoff error
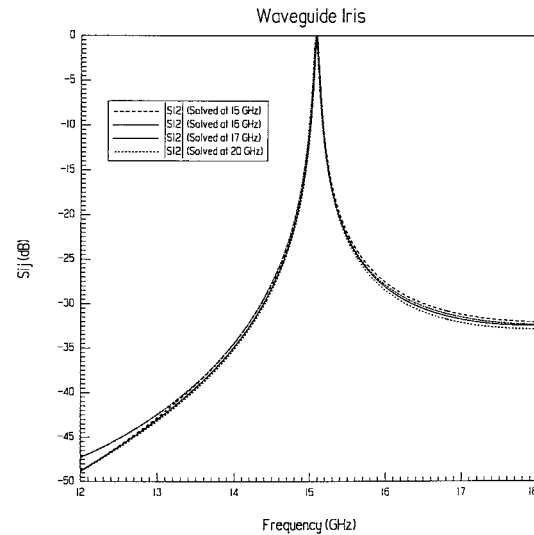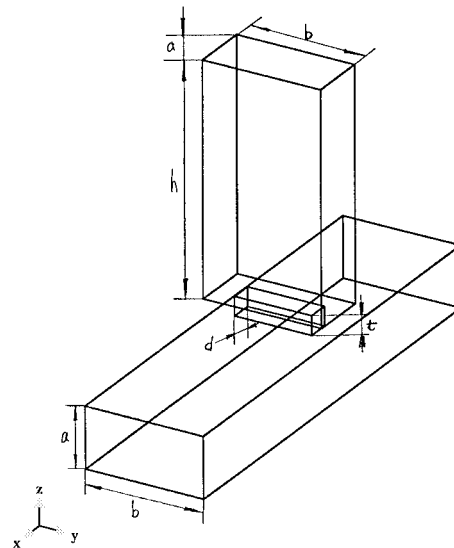
occurs. Although the matrix residue is often less than 10^{-6} or -120 dB when it is directly decomposed, it is observed that this method provides accurate scattering parameters for a large number of practical structure even when the matrix residue is as large as -20 dB. This is clearly illustrated in Fig. 13 where ten poles are used in the Padé approximation.

The structure in Fig. 14 has a resonance around 15 GHz. To demonstrate the robustness of the method, the problem is solved at several center frequencies. Fig. 13 shows a typical matrix residue versus frequency plot for the case when the matrix is factored using ten poles at the center frequency of 15 GHz. Fig. 15 shows that the center frequency has almost no effect on the spectral response even though the rational functions representing the system are different. This is an important property of the s-domain approach: one is not required to specify the solution frequency. Rather, one must satisfy the loose requirement that the center frequency should be in the bandwidth of interest.
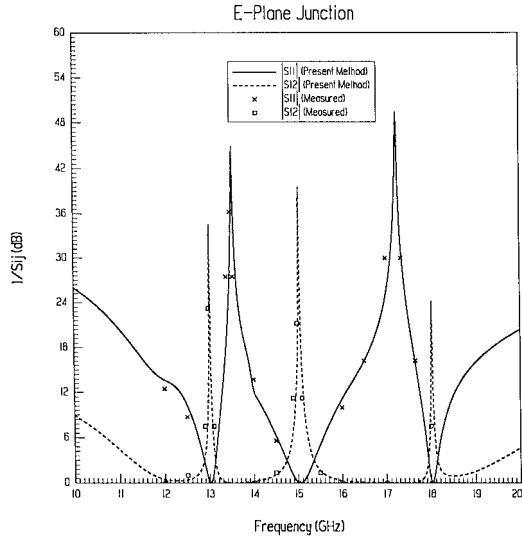
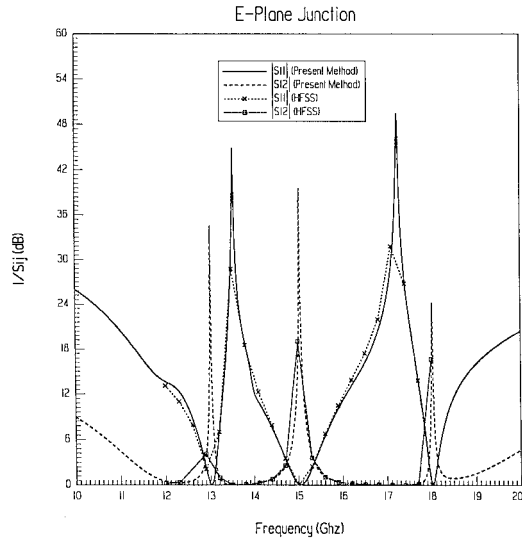Fig. 17. Computed fast-sweep results for the structure of Fig. 16 compared with measured results in [24].

Fig. 18. Computed fast-sweep results for the structure of Fig. 16 compared with conventional discrete frequency sweep results from HFSS.

The last finite-element example is the E-plane slot coupled T-junction in a rectangular waveguide, as shown in Fig. 16. This T-junction exhibits several sharp resonances between 12 and 18 GHz, indicating the existence of several dominant poles in this frequency range. Applying the s-domain solution procedure at a single frequency range does not capture all of the resonances accurately. Thus, we employ CFH to combine the Taylor-series expansions at multiple frequencies to produce a single rational function for the entire bandwidth, as given in (6). We solve the T-junction in Fig. 16 for ten derivatives at each of the three different frequencies at 13.2, 15.0, and 17.2 GHz. The resulting rational function has 15 poles. Fig. 17 compares the computed s-parameter spectra response with the measured results, as given by Sieverding *et al.* [25, Fig. 6(b)]. The agreement between computed and measured results is excellent. Also shown in Fig. 18 are discrete frequency solutions obtained by solving the problem at 21 discrete frequencies.
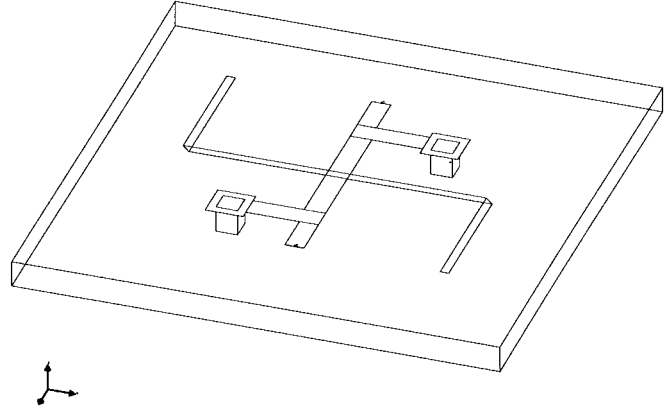

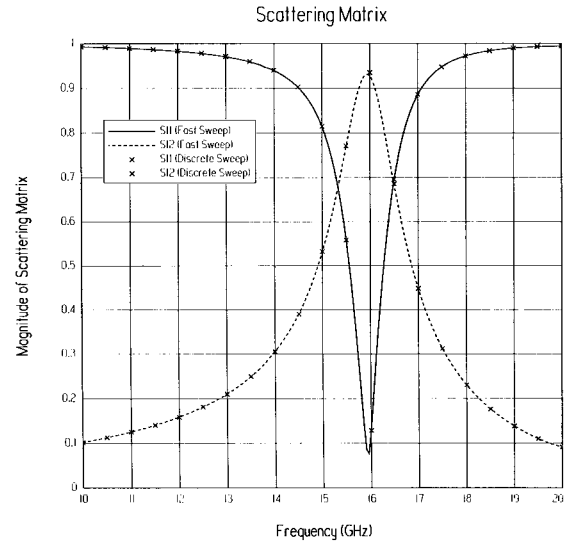Fig. 19. A low-pass microstrip filter using grounded vias.

Fig. 20. Comparison of ALPS results with the conventional discrete frequency sweep in Strata.

While this discrete solution is accurate at the 21 computed frequencies, the s-domain method clearly produces a far better and more complete result.

The next example demonstrates the use of fast sweep techniques for an integral-equation solver. The problem is the low-pass filter structure, shown in Fig. 19. This was analyzed using Strata, a full-wave boundary-element code with ALPS-based fast-frequency sweep. The results of the fast sweep are compared with a discrete frequency sweep (X's), shown in Fig. 20. The agreement is quite good across the entire frequency band.

Another low-pass filter is shown in Fig. 21(a). The computed scattering parameters were modeled with rational functions of 16–18 poles. A comparison of the sweep results with the reduced-order model is shown in Fig. 21(b).

A two-port equivalent circuit model for the structure was then generated; this was connected to a nonlinear metal–oxide–semiconductor (MOS) inverter driver. The transmitted and reflected pulses from a transient simulation are shown in Fig. 22.
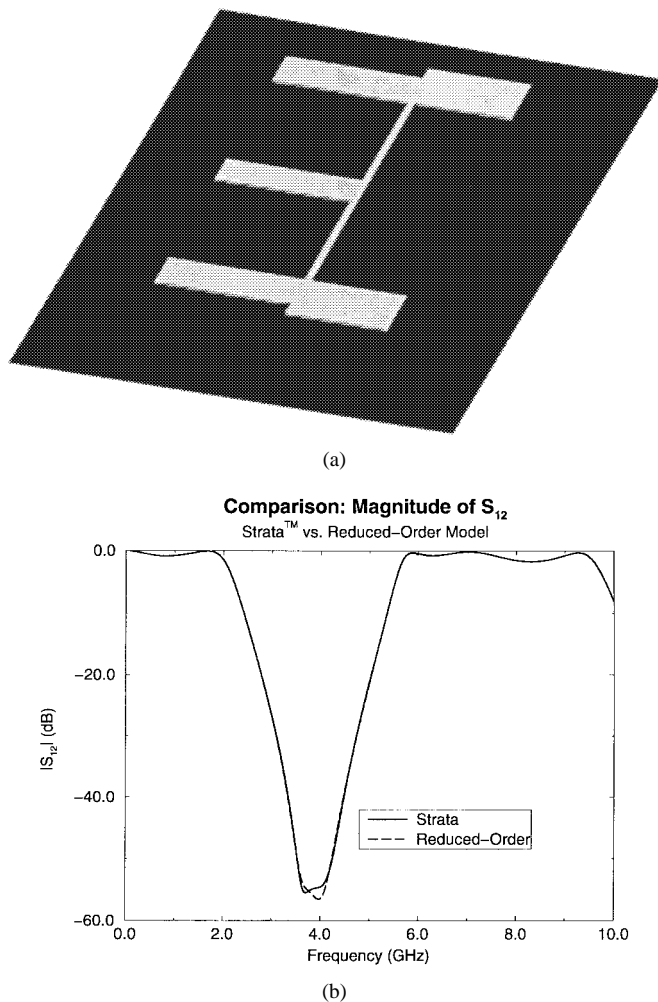
(a)

(b)

Fig. 21.   (a) Chebyshev third-order low-pass filter structure. (b) Comparison of Strata's frequency response (computed by fast sweep) and the reduced-order model.

(a)

(b)

Fig. 22.   Transient simulation results from HSPICE analysis of the combined MOS driver and reduced-order model.

The second example [Fig. 23(a)] is taken from printed circuit-board design. It consists of two symmetrical wires used in a differential signaling scheme; the wires make a 90° bend, which includes a transition from an x-routing layer to a y-layer through a pair of vias. There are ground planes above and below the structure. We wish to investigate the crosstalk between the undesired common mode (even mode) of propagation and the signal-carrying differential mode (odd mode). The structure was analyzed by Ansoft HFSS, using both a standard discrete frequency sweep and fast frequency-sweep techniques; the modal S-parameters were converted into circuit-based parameters for even and odd modes and then fitted by reduced-order models. The point-by-point frequency sweep (100 points) took 2.5 h of CPU time on a DEC Alpha 3000/800 workstation, while the fast frequency sweep took less than 0.2 CPU h. Plots of the near- and far-end crosstalk magnitudes are shown as a function of frequency in Fig. 23(b). In addition, we have computed the time-domain crosstalk waveforms for the structure, assuming that input pulses with 0.1-ns rise times drive the even and odd modes. Plots of these waveforms are given in Fig. 24(a). This information could be used to create "design rules" for the maximum
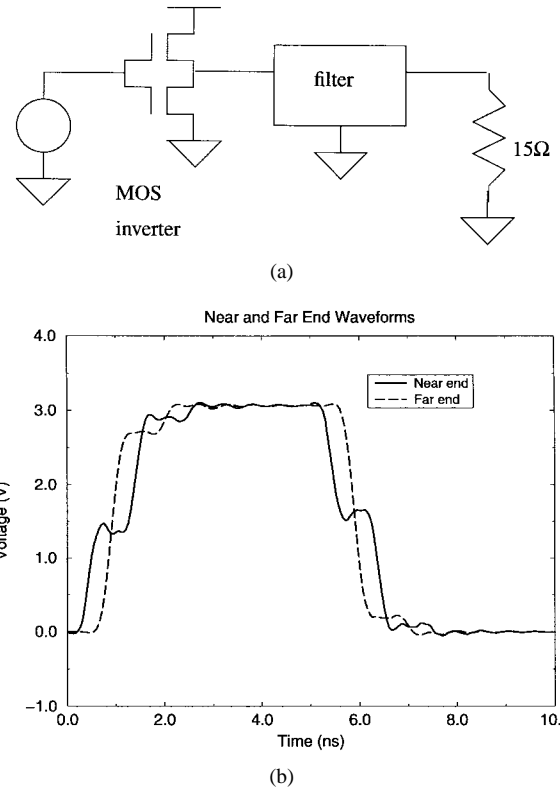
number of right-angle bends allowed for a certain maximum crosstalk.

Also shown [Fig. 24(b)] are the signal waveforms at the near and far ends. Notice that the waveforms predict a delay of approximately 0.1 ns from input to output. This is consistent with the relative dielectric constant ($\varepsilon = 4$, a velocity of 1.5×10^8 m/s) and the total distance traveled (about 16 mm).

X. Conclusions

Fast frequency-sweep methods provide a powerful tool for characterizing the electromagnetic behavior of structures that are intended to operate over a broad frequency band, or whose time-domain characteristics are important. Reduced-order models can be generated with a computational cost, which is small compared to the field analysis at a single frequency. In this paper, we have demonstrated how fast sweep techniques may be applied to both finite-element and integral-equation formulations of the full-wave electromagnetic-analysis problem.

For the finite-element approach, the transfinite-element formulation of Maxwell's equations was coupled with AWE to compute the spectral response efficiently. Speed improvements of ten times or more over the traditional approach were obtained when analyzing typical microwave structures. In many cases, the spectral response over a wide bandwidth was accurately obtained by solving the problem at a single frequency and performing the AWE procedure. The solution is typically most accurate near the center frequency of the series expansion. However, it becomes less accurate as the frequency
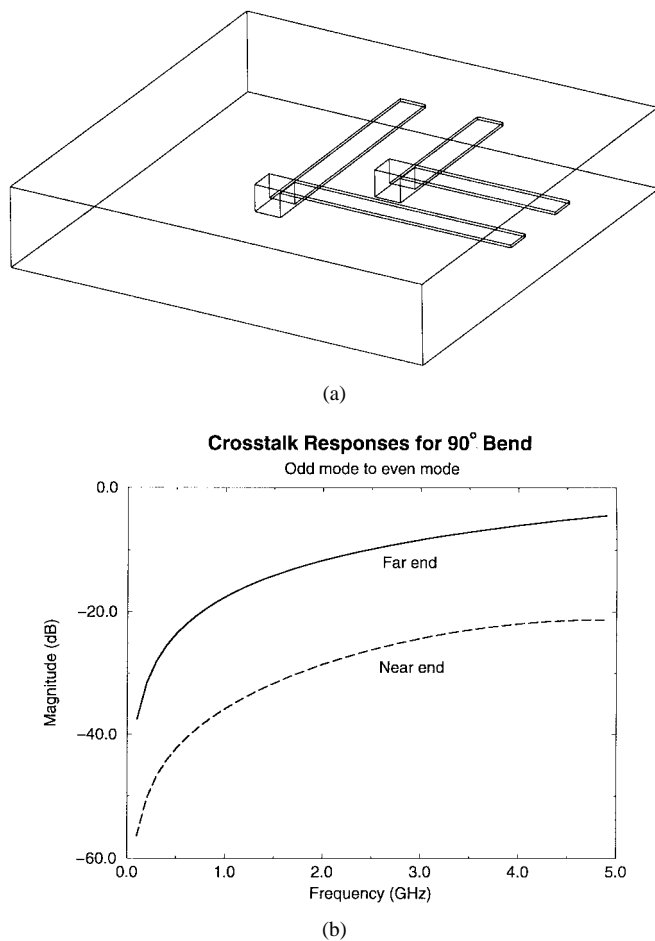
(a)

Fig. 23.   (a) Three-dimensional printed circuit-board structure including vias and 90° bend. (b) Simulated far-end crosstalk response between odd and even modes.
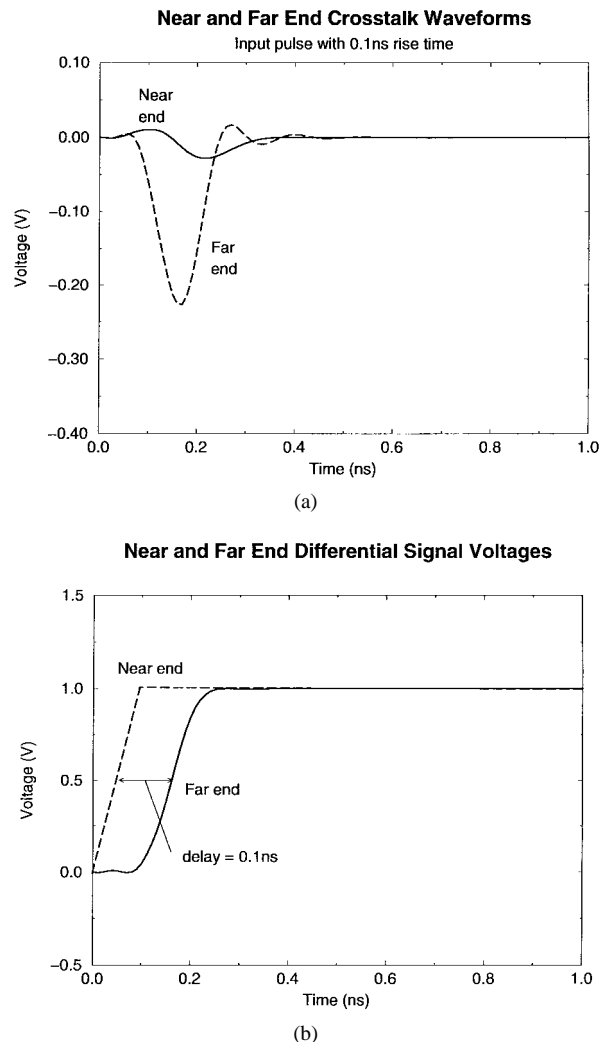

(a)

(b)

Fig. 24.   (a) Time-domain crosstalk waveforms at the input (near) and output (far) ports. (b) Time-domain differential-signal waveforms at the near and far ends.

departs from the expansion point. The range of validity is problem dependent. If the frequency response of the structure is required over a broad band, additional solutions at different frequencies may be performed and then combined together using CFH.

Alternatively, one may use the ALPS procedure, which adaptively solves at the frequency points of maximum error using the Lanczos algorithm with selective orthogonalization. The procedure is highly reliable and efficient. Typically, it needs fewer than five adaptive solutions. As shown in our test cases, excellent agreement is obtained between ALPS solutions and direct solutions. The ALPS procedure also makes it possible to apply fast sweep techniques to integral-equation formulations of the electromagnetics problem. For these formulations, the complicated frequency dependence of the matrices would prevent the use of the AWE of Lanczos procedures.

We have also explored the problems of efficient time-domain and mixed linear/nonlinear simulation. Reduced-order circuit models were derived from the fast sweep results; these allowed us to characterize the time-domain behavior of electromagnetic structures in the presence of nonlinear loading. Since the simulation of the nonlinear problem is carried out in a circuit-level tool such as SPICE, the analysis is orders of

magnitude faster than can be achieved in a field simulator. This permits the user to change the nonlinear-device characteristics and resimulate without long delays.

REFERENCES

[1] A. Taflove, *Computational Electrodynamics: The Finite-Difference Time-Domain Method.* Norwood, MA: Artech House, 1995.
[2] L. T. Pillage and R. A. Rohrer, "Asymptotic waveform evaluation for timing analysis," *IEEE Trans. Computer-Aided Design*, vol. 9, pp. 352–366, Apr. 1990.
[3] V. Raghavan, R. A. Rohrer, L. T. Pillage, J. Y. Lee, J. E. Bracken, and M. M. Alaybeyi, "AWE-Inspired," in *Proc. IEEE Custom IC Conf.*, San Diego, CA, May 1993, pp. 18.1.1–18.1.8.
[4] J. E. Bracken, V. Raghavan, and R. A. Rohrer, "Simulating distributed elements with asymptotic waveform evaluation," *IEEE Int. Microwave Symp.*, Albuquerque, NM, 1992, pp. 1337–1340.
[5] E. Chiprout and M. S. Nakhla, *Asymptotic Waveform Evaluation and Moment Matching for Interconnect Analysis.* Norwell, MA: Kluwer, 1994.

[6] P. Feldman and R. W. Freund, "Efficient linear circuit analysis by Padé approximation via the Lanczos process," *IEEE Trans. Computer-Aided Design*, vol. 14, pp. 639–649, May 1995.

[7] E. H. Newman, "Generation of wide-band data from the method of moments by interpolating the impedance matrix," *IEEE Trans. Antennas Propagat.*, vol. AP-30, pp. 1820–1824, Dec. 1988.

[8] K. Kottapalli, T. K. Sarkar, Y. Hua, E. K. Miller, and G. J. Burke, "Accurate computation of wide-band response of electromagnetic systems utilizing narrow-band information," *IEEE Trans. Microwave Theory Tech.*, vol. 39, pp. 682–687, Apr. 1991.

[9] A. E. Ruehli, H. Heeb, J. E. Bracken, and R. Rohrer, "Three-dimensional circuit-oriented electromagnetic modeling for VLSI interconnects," presented at the Proc. IEEE Int. Conf. Computer Design, Chicago, IL, 1992.

[10] X. Yuan and Z. Cendes, "A fast method for computing the spectral response of microwave devices over a broad bandwidth," in *Proc. APS/URSI Int. Symp.*, Ann Arbor, MI, June 1993, p. 196.

[11] D.-K. Sun, "ALPS—An adaptive Lanczos–Padé approximation for the spectral solution of mixed-potential integral equations," in *USNC/URSI Radio Sci. Meeting Dig.*, July 1996, p. 30.

[12] G. A. Baker, Jr., *Essentials of Padé Approximants.* New York: Academic, 1975.

[13] X. Huang, V. Raghavan, and R. A. Rohrer, "AWEsim: A program for the efficient analysis of linear(ized) circuits," in *IEEE Int. Conf. Computer-Aided Design*, Santa Clara, CA, Nov. 1990, pp. 534–537.

[14] C. Lanczos, "An iteration method for the solution of the eigenvalue problem of linear differential and integral operators," *J. Res. Natl. Bur. Stand.*, vol. 45, pp. 255–282, 1950.

[15] B. N. Parlett and D. S. Scott, "The Lanczos algorithm with selective orthogonalization," *Math. Comput.*, vol. 33, no. 145, pp. 217–238, 1979.

[16] B. Nour-Omid, B. N. Parlett, and R. L. Taylor, "Lanczos versus subspace iteration for solution of eigenvalue problems," *Int. J. Numer. Methods Eng.*, vol. 19, pp. 859–871, June 1983.

[17] Z. J. Cendes and J.-F. Lee, "The transfinite element method for modeling MMIC devices," *IEEE Trans. Microwave Theory Tech.*, vol. 36, pp. 1639–1649, Dec. 1988.

[18] J.-F. Lee, D.-K. Sun, and Z. J. Cendes, "Tangential vector finite elements for electromagnetic field computation" *IEEE Trans. Magn.*, vol. 27, pp. 4032–4035, Sept. 1991.

[19] Z. J. Cendes, "Vector finite elements for electromagnetic field computation," *IEEE Trans. Magn.*, vol. 27, pp. 3958–3966, Sept. 1991.

[20] C. Hwang and Y.-C. Lee, "Multifrequency Padé approximation via Jordan continued-fraction expansion," *IEEE Trans. Automat. Cont.*, vol. 34, pp. 444–446, Apr. 1989.

[21] L. W. Nagel, "SPICE2: A computer program to simulate semiconductor circuits," Univ. California Berkeley Electron. Res. Labs., memo UCB/ERL M520, May 1975.

[22] T. L. Quarles, "Analysis of performance and convergence issues for circuit simulations," Univ. California Berkeley Electron. Res. Labs, memo UCB/ERL M89/42, Apr. 1989.

[23] F. Giannini, G. Bartolucci, and M. Ruggieri, "Equivalent circuit models for computer-aided design of microstrip rectangular structures," *IEEE Trans. Microwave Theory Tech.*, vol. 40, pp. 378–388, Feb. 1992.

[24] R. Mansour, R. S. K. Tong, and R. H. Macphie, "Simplified description of the field distribution in finlines and ridge waveguides and its application to the analysis of E-plane discontinuities," *IEEE Trans. Microwave Theory Tech.*, vol. 36, pp. 1825–1832, Dec. 1988.

[25] T. Sieverding and F. Arndt, "Field theoretic CAD of open or aperture matched T-junction coupled rectangular waveguide structures," *IEEE Trans. Microwave Theory Tech.*, vol. 40, pp. 353–362, Feb. 1992.

[26] J. R. Mosig and F. E. Gardiol, "General integral equation formulation for microstrip antennas and scatterers," *Proc. Inst. Elect. Eng.*, vol. 132, pt. H, pp. 424–432, Dec. 1985.

[27] S. M. Rao, D. R. Wilton, and A. W. Glisson, "Electromagnetic scattering by surfaces of arbitrary shape," *IEEE Trans. Antennas Propagat.*, vol. AP–30, pp. 409–418, May 1982.

[28] L. M. Silveira, M. Kamon, and J. White, "Efficient reduced-order modeling of frequency-dependent coupling inductances associated with 3-D interconnect structures," in *Proc. 32nd IEEE/ACM Design Automation Conf.*, San Francisco, CA, June 1995, pp. 376–380.

[29] V. Raghavan, J. E. Bracken, and R. A. Rohrer, "AWESpice: A general tool for the accurate and efficient simulation of interconnect problems," in *Proc. 29th IEEE/ACM Design Automation Conf.*, Anaheim, CA, June 1992, pp. 87–92.

J. Eric Bracken (S'87–M'92) received the B.S. (with honors), M.S., and Ph.D. degrees in electrical and computer engineering from Carnegie-Mellon University, Pittsburgh, PA, in 1987, 1989 and 1994, respectively.

In 1992, he cofounded Performance Signal Integrity, the first company to commercialize AWE technology. He has held positions at AT&T Bell Laboratories, Eastman Kodak, Motorola, Integrated Silicon Systems, and Carnegie-Mellon University. He is currently the Group Leader for signal integrity product R&D at Ansoft Corporation, Pittsburgh, PA. He has written several journal and conference papers, as well as the ANSI/EIA IBIS 2.1 package electrical model specification. He holds one U.S. patent in the area of circuit simulation. His research interests are in circuit theory, circuit simulation, reduced-order modeling techniques, and parasitic circuit extraction via field simulation.

Din-Kow Sun (M'89) was born in Taipei, Taiwan, R.O.C., in 1956. He received the B.S. degree from National Taiwan University, Taiwan, R.O.C., in 1978, and the Ph.D. degree from Carnegie-Mellon University, Pittsburgh, PA, in 1984, all in physics.

He was a Research Associate in the Department of Electrical and Computer Engineering, Carnegie-Mellon University, from 1984 to 1986. Since 1986, he has been a Research Engineer at Ansoft Corporation, Pittsburgh, PA. His current research projects include the applications of Lanczos and multigrid methods in computing the spectral response of microwave devices over a broad bandwidth.

Zoltan J. Cendes (S'67–M'73), received the M.S. and Ph.D. degrees in electrical engineering from McGill University, Montreal, P.Q., Canada.

He is Founder and Chief Technology Officer of Ansoft Corporation, Pittsburgh, PA. He serves as the Technical Leader of Ansoft's research and development, where he is responsible for managing the company's product and technology research. Most notably, he is responsible for developing the theory behind the HFSS, originally marketed for Ansoft by the Hewlett-Packard Company, and now marketed directly by Ansoft. He is a professor of electrical and computer engineering at Carnegie-Mellon University, Pittsburgh, PA. Prior to joining the faculty of Carnegie-Mellon, he served as Associate Professor of electrical Engineering at McGill University, Montreal, P.Q., and as Adjunct Associate Professor of electrical engineering at Union College, Schenectady, N.Y. His previous experience includes six years with the General Electric Corporation, first in the Large Steam Turbine Generator Division and then in the Corporate Research and Development Center. He is on the editorial board of the MIMICAD Journal and has served on the International Steering Committee of the COMPUMAG Conference.

Dr. Cendes is a member of the MTT Technical Committee on Computer-Aided Design and is a past chairman of the IEEE Conference on Electromagnetic Field Computation.